Kasetsart J. (Nat. Sci.) 48 : 150 - 166 (2014)

Integrating an Input Shaper with a Quantitative-Feedback-Theory-Based Controller to Effectively Reduce Residual Vibration in Slewing of a Two-Staged Pendulum with Uncertain Payload

Withit Chatlatanagulchai[1,*], Puwadon Poedaeng[1] and Peter Heinrich Meckl[2]

ABSTRACT

In this study, a control system was proposed consisting of an outside-of-the-loop input shaper and a feedback controller based on quantitative feedback theory. The input shaper convolves the reference input with a properly designed impulse sequence to generate a shaped reference input that reduces the excitation in the system's modal frequencies, resulting in less residual vibration. Recently, the input shaper has been placed inside-of-the-loop to attenuate noise-induced vibration under hard nonlinearity. However, this setting cannot reduce the vibrations induced from plant-input and plant-output disturbances as well as from plant model uncertainty. A controller was designed to meet various disturbance rejection specifications, when plant uncertainty is also taken into account. The input shaper was then designed using the closed-loop natural frequencies and damping. Together, the proposed control system could effectively reduce residual vibrations especially those induced from disturbances and uncertainty. The control system was applied to a two-staged pendulum where all masses were lumped together to create a simplified model used in controller design, and the inertia forces of both links and payload were treated as plant-input disturbance. Simulation and experimental results indicated that the control system was very effective in residual vibration reduction in the presence of uncertainty and disturbances.

Keywords: vibration reduction, two-staged pendulum, input shaping, quantitative feedback theory

INTRODUCTION

The input shaping technique, proposed by Singer and Seering (1989, 1990) convolves the reference input with a properly designed impulse sequence. The impulse sequence is designed such that all impulse responses cancel one another producing vibration-free movement. By inspecting its frequency spectrum, the resulting shaped reference input practically has low spectrum energy around the closed-loop system's natural frequencies, which explains how the low residual vibration is obtained. The input shaping technique compared favorably with conventional filters, such as low-pass or notch filters, as was presented by Singhose *et al.* (1995).

Recently, some research has investigated placing the input shaper inside-of-the-loop, a so-called closed-loop signal shaper (CLSS.) Huey *et al.* (2008) reported that the CLSS can reduce noise-induced vibration and alleviate the detrimental effects caused by hard nonlinearity such as saturation and rate limit. However, a CLSS is not suitable for eliminating vibrations induced

1 Department of Mechanical Engineering, Faculty of Engineering, Kasetsart University, Bangkok 10900, Thailand.
2 School of Mechanical Engineering, Purdue University, West Lafayette, IN 47907-2088, USA.
* Corresponding author, e-mail: fengwtc@ku.ac.th

Received date : 29/03/11 Accepted date : 05/09/13

by plant-input and plant-output disturbances as well as by plant model uncertainty. Staehlin and Singh (2003) used the structure of the internal model controller for the closed-loop control without results on robustness. Kapila *et al.* (1999) applied a closed-loop controller based on the linear matrix inequality to a simulation problem. However, the controller is quite complicated and its use in practice is still limited. Zolfagharian *et al*. (2013) used a proportional-derivative (PD) and an iterative learning controller in the feedback loop. A genetic algorithm was used to adjust their gains to provide robustness. Huey and Singhose (2010a) used root locus to show that the closed-loop system, consisting of the input shaper placed inside-of-the-loop and a simple P, PID or lead controller, is susceptible to instability. Stergiopoulos and Tzes (2010) applied an H_∞ robust controller to the feedback loop with the input shaper placed inside. The controller addresses the uncertainty of the plant transfer function's denominator, which ensures accurate tracking. Pai (2012) independently used a sliding mode controller in the feedback loop to make the closed-loop system behave like a reference model. An input shaper was then designed to suppress vibration of the reference model. Huey and Singhose (2010b) used a PD in the feedback loop. They concurrently designed the PD gains and the input shaper parameters for a simple plant by taking into account limits on the allowable overshoot, residual vibration and actuator effort.

Because vibrations induced by disturbances and uncertainty are substantial, it is appropriate to put a controller inside-of-the-loop to attenuate the disturbances when uncertainty is present. Then, the input shaper can be placed outside-of-the-loop to create a shaped reference input for the resulting closed-loop system. The ability of the controller in attenuating the disturbances with pre-specified performance is vital for the proposed setting.

Quantitative feedback theory (QFT) is a frequency-based controller design technique that was devised by Horowitz (1959) over fifty years ago. The controller design is performed mainly on the Nichols chart, where at a specific frequency, the plant is viewed as an area containing possible plant variations. The design on this so-called plant template ensures robustness over all plant model uncertainties. Parameters, such as disturbances and noise rejection as well as tracking and control effort, can be pre-specified to guarantee that the closed-loop system will behave as desired.

QFT has recently become practical with the invention of some computer-aided-design packages (Houpis and Lamont, 1992; Sating, 1992; Borghesani, 1993) and has been implemented in various challenging applications such as the control of a continuous stirred tank reactor (Houpis and Chandler, 1992) the idle speed control of an automotive fuel-injected engine (Franchek and Hamilton, 1997) an F-16 flight control system (Phillips *et al.*, 1995), a waste water treatment control system (Garcia-Sanz and Ostolaza, 2000), large wind turbine control systems (Torres and Garcia-Sanz, 2004) positioning a pneumatic actuator (Karpenko and Sepehri, 2004) and the coordinated control of formation flying spacecraft (Garcia-Sanz and Hadaegh, 2004).

The objective of this paper was to integrate these two very practical techniques—namely, the input shaping technique and the QFT-based controller—to create a control system that can effectively reduce residual vibrations induced from various sources such as reference input, plant-input and plant-output disturbances, sensor noise and plant uncertainty.

A two-staged pendulum was used as an example application. The pendulum possesses a quite complicated mathematical model, which may not be suitable for the controller design. Interestingly, by lumping all masses together and by treating the inertia forces from swinging motions of the links and the payload as plant-input disturbances, a simple second-order model that replicates the dynamics of the complicated model of the pendulum was obtained.

A QFT-based controller was designed to attenuate the effect from the disturbance above. It was shown that the controller also attenuates the effect from noise and plant-output disturbance. Following the controller design, an input shaper was designed using the closed-loop natural frequencies and damping. The overall control system was able to greatly attenuate the residual vibration under point-to-point motion. The setting has proved to be very practical and rather convenient. Since the input shaper can perform in real-time, the method is also suitable for attenuating the vibration of any arbitrary motion command such as that given by a human operator.

MATERIALS AND METHODS

Input shaping basics

More detail on the input shaping basics can be found in Singer and Seering (1989) who originated this technique.

For a one-degree-of-freedom, under-damped, unforced, linear system, two impulses $\hat{F}_1$ and $\hat{F}_2$ may produce responses as shown in Figure 1a. With proper design, the two responses can cancel each other leaving zero oscillation as shown in Figure 1b.

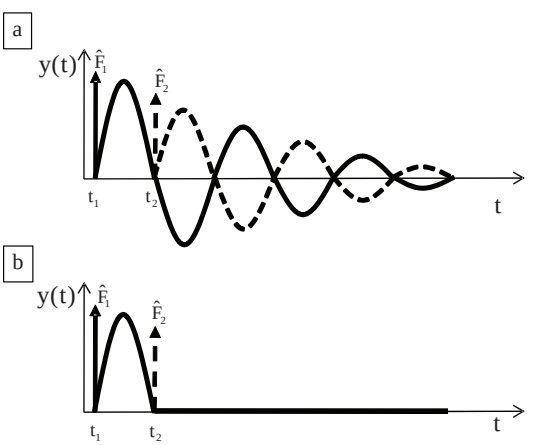

Figure 1 System response of two impulses $\hat{F}_1$ and $\hat{F}_2$ for a one-degree-of-freedom, under-damped, unforced, linear system over time (t): (a) Without cancellation; and (b) With cancellation.

Let $t_1 = 0$ and $\hat{F}_1 = 1$ and set the amplitude of the summation of the two impulse responses to zero at a time t_2 to obtain Equation 1:

$$\hat{F}_2 = e^{-\frac{\zeta\pi}{\sqrt{1-\zeta^2}}} \text{ and } t_2 = \frac{\pi}{\omega_n\sqrt{1-\zeta^2}}, \quad (1)$$

where ζ and ω_n are the damping ratio and natural frequency of the system, respectively.

To reduce the sensitivity of the vibration reduction to variations in the system damping ratio and the natural frequency, the derivatives of the summation of the responses, with respect to the natural frequency and the damping ratio, are set to zero yielding the magnitude and time of the third impulse as Equation 2:

$$\hat{F}_3 = e^{-\frac{2\zeta\pi}{\sqrt{1-\zeta^2}}} \text{ and } t_3 = \frac{2\pi}{\omega_n\sqrt{1-\zeta^2}}. \quad (2)$$

For a system with n modes, n impulse sequences can be obtained in a similar manner, where one natural frequency and one damping ratio are considered at a time.

The impulse sequences developed can be applied to the closed-loop system as shown in Figure 2. The input shaper block represents the on-line convolution operation between the impulse sequences and an arbitrary reference input. The natural frequencies and damping ratios used in designing the impulse sequence are those of the closed-loop system.

The output of the input shaper practically has a low spectrum energy around the closed-loop

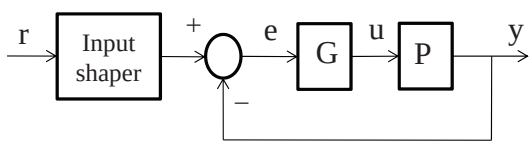

Figure 2 Closed-loop-system block diagram with an input shaper (G is a controller, P is a plant, r, e, u and y are the reference input, error, plant input and plant output, respectively).

natural frequencies; therefore, the resonances can be reduced resulting in less residual vibrations.

Quantitative feedback theory basics

QFT can be applied to feedback systems as depicted in Figure 3.

Frequency-domain specifications are described in terms of inequalities on the system's transfer functions from some inputs to some outputs. For example, the plant-input disturbance rejection specification is given by Equation 3:

$$\left|y / d_I\right| = \left|P_{dI} P / \left(1 + PGH\right)\right| < \delta_{dI}, \qquad (3)$$

the plant-output disturbance rejection specification is given by Equation 4:

$$\left|y / d_O\right| = \left|P_{dO} / \left(1 + PGH\right)\right| < \delta_{dO}, \qquad (4)$$

and the tracking specification is given by Equation 5:

$$\alpha \le \left|PGF / \left(1 + PGH\right)\right| \le \beta, \qquad (5)$$

where P represents a linear plant in a set {P} that contains all possible variations due to uncertainties; H represents the sensor transfer function; controller G and prefilter F are to be synthesized to meet robust stability and closed-loop specifications; d_I and d_O are disturbances at plant input and output, respectively, together with their transfer functions P_{dI} and P_{dO}, respectively; y is the plant output; δ_{dI} and δ_{dO} are two small numbers; and α and β are tracking lower and upper bounds. Other specifications such as noise rejection, model matching and control effort can also be specified.

For one frequency ω and one frequency-domain specification, a bound can be computed on the Nichols chart. The controller G and the prefilter F must later be designed by loop shaping to satisfy these bounds to ensure that all pertaining specifications are met. QFT design steps will be elaborated in the next section when the controller and the prefilter are designed for the two-staged pendulum. However, more details on QFT-based controller design are available in Chatlatanagulchai *et al*. (2008) and in some excellent textbooks (Horowitz, 1993; Yaniv, 1999; Sidi, 2001; Houpis *et al.*, 2005).

Simulation of a two-staged pendulum

To demonstrate the performance of the proposed control system, a two-staged pendulum

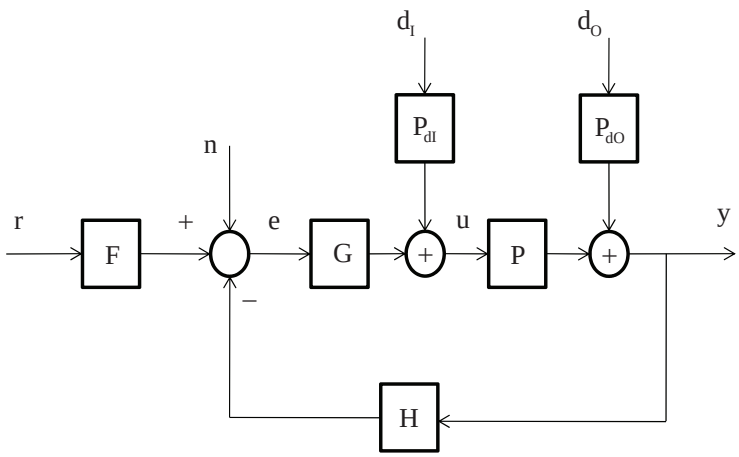

Figure 3 Applicable feedback system. Plant P represents a linear plant in a set {P} that contains all possible variations due to uncertainties. H represents sensor transfer function. Controller G and prefilter F are to be synthesized to meet robust stability and closed-loop specifications; d_I and d_O are disturbances at plant input and output, respectively, together with their transfer functions P_{dI} and P_{dO}, respectively; and n, r, e, u and y are the sensor noise, reference input, error, plant input and plant output, respectively.

was used as an example. The QFT-based controller design and the input shaper design along with their simulation results and discussions are given in this section whereas the experimentation details will be presented in the next section.

Obtaining a control-design model

The aim was to design a control system for point-to-point movement of a two-staged pendulum in the vertical plane whose diagram is given in Figure 4. One of the potential applications of this pendulum is the object-moving crane. The pendulum system consists of a slider, two rigid links and an uncertain payload. A linear motor drives the pendulum system. The objective is to move the payload from point to point, back and forth, as fast as possible. This can be achieved only when the oscillations of the links are minimized.

From Figure 4, the pendulum has three degrees of freedom namely x, θ_1 and θ_2, where $\ddot{s}$ represents payload linear acceleration. Using Lagrange's method to find its equations of motion, a set of three equations (summarized as Equation 6) is obtained:

$$\begin{aligned}
&m\ddot{x}+m_1\left(\ddot{x}-\frac{l_1}{2}\ddot{\theta}_1\right)+m_2\left(\ddot{x}-l_1\ddot{\theta}_1-\frac{l_2}{2}\ddot{\theta}_2\right)+m_p\left(\ddot{x}-l_1\ddot{\theta}_1-l_2\ddot{\theta}_2\right)\\
&-m_1\left(\ddot{x}-\frac{l_1}{2}\ddot{\theta}_1\right)\frac{l_1}{2}+J_1\ddot{\theta}_1-m_2\left(\ddot{x}-l_1\ddot{\theta}_1-\frac{l_2}{2}\ddot{\theta}_2\right)l_1+J_2\left(\ddot{\theta}_1+\ddot{\theta}_2\right) = F-c\dot{x},\\
&-m_p\left(\ddot{x}-l_1\ddot{\theta}_1-l_2\ddot{\theta}_2\right)l_1+J_p\left(\ddot{\theta}_1+\ddot{\theta}_2\right)+m_1g\frac{l_1}{2}\sin\theta_1+m_2gl_1\sin\theta_1\\
&+m_2g\frac{l_2}{2}\sin\left(\theta_1+\theta_2\right)+m_pgl_1\sin\theta_1+m_pgl_2\sin\left(\theta_1+\theta_2\right) = -c_1\dot{\theta}_1,\\
&-m_2\left(\ddot{x}-l_1\ddot{\theta}_1-\frac{l_2}{2}\ddot{\theta}_2\right)\frac{l_2}{2}+J_2\left(\ddot{\theta}_1+\ddot{\theta}_2\right)-m_p\left(\ddot{x}-l_1\ddot{\theta}_1-l_2\ddot{\theta}_2\right)l_2\\
&+J_p\left(\ddot{\theta}_1+\ddot{\theta}_2\right)+m_2g\frac{l_2}{2}\sin\left(\theta_1+\theta_2\right)+m_pgl_2\sin\left(\theta_1+\theta_2\right) = -c_2\dot{\theta}_2.
\end{aligned} \tag{6}$$

where the parameters are defined in Table 1.

It should be noted that, in deriving the equations above, the assumption is made that the centers of gravity of both links and the payload have only horizontal velocity. Due to the small amount of link movement in this gantry-like application, the terms due to the vertical movement are neglected to avoid complication. For systems where the assumption of small-signal linearization is inappropriate, the linear time invariant equivalent method for large signals presented in Horowitz (1993) can be used. All parameters and their values are given in Table 1.

The equations of motion above are nonlinear, which is an impediment to the use of

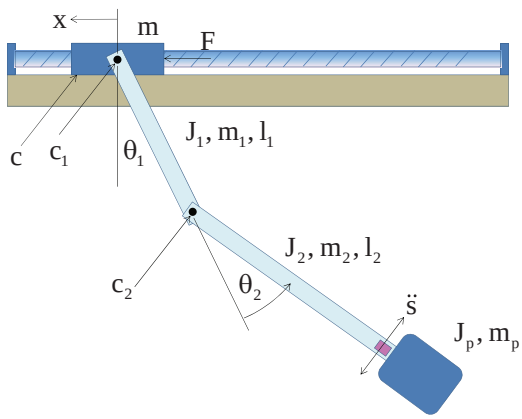

Figure 4 Diagram of a two-staged pendulum. The pendulum has three degrees of freedom namely x, θ_1, and θ_2, where $\ddot{s}$ represents payload linear acceleration, and the other parameters are defined in Table 1.

Table 1 Parameters and their values for the two-staged pendulum based on the actual experimental hardware.

Parameter	Description	Value
J_1, J_2, J_p	Links and payload mass moment of inertia about the center of gravity (kg.m^2)	7.5×10^{-4}, 0.0082, 0.001
m, m_1, m_2, m_p	Slider, links, and payload mass (kg)	0.1, 0.1, 0.2, 0.2
l_1, l_2,	Links length (m)	0.3, 0.7
c, c_1, c_2,	Slider and links friction coefficients (kg.s^{-1})	1, 0.01, 0.01
F	Push force from screw (N)	

QFT. It is used as a true model to represent the actual pendulum in the simulation.

For controller design, a simpler model that can imitate the true model closely is needed. The idea is to move all masses together as one rigid body, so that then the oscillation of the links and the payload is viewed as a plant-input disturbance, which will be attenuated by the controller. When all masses are lumped together, a simple second-order model is obtained (Equation 7):

$$M\ddot{x} + c\dot{x} = F + O_x, \quad (7)$$

where $M = m + m_1 + m_2 + m_p$ and O_x is the force disturbance resulting from oscillations of the links and payload and the free-body diagram of all the horizontal forces in Figure 5 results in

$$O_x = m_1\ddot{\theta}_1\frac{l_1}{2} + m_2\left(\ddot{\theta}_1 l_1 + \ddot{\theta}_2\frac{l_2}{2}\right) + m_p\left(\ddot{\theta}_1 l_1 + \ddot{\theta}_2 l_2\right).$$

It can be shown that this simplified model with disturbance is identical to the true model when $\sin\theta \approx \theta$.

QFT-based controller design

The control system, shown in Figure 6, comprises an outside-of-the-loop input shaper, a QFT-based controller (G) and a QFT-based prefilter (F). The QFT-based control system can be designed so that the closed-loop system is robust against uncertainty in the plant model as well as being able to reject disturbances d_I and d_O. In this section, the QFT-based controller design is presented whereas the input shaper design will be given in the next section.

The control-design plant model is a simple second-order model given in Equation 7. Comparing Figure 6 with Equation 7, the output *y* is the slider displacement *x* ; the plant-input disturbance d_I is the inertia force O_x; the plant-output disturbance d_O is, for example, ground vibration; and the control input *u* is the force acting on the sliding mass.

The design objective is to have the displacement *x* track the reference input r as close as possible whereas the inertia force disturbance O_x from swinging of the links and payload, is attenuated. It should be noted that the actual objective is tracking of the payload not the slider. However, by attenuating the swinging disturbance, and later by applying the input shaper to the closed-loop system, the swinging will be greatly

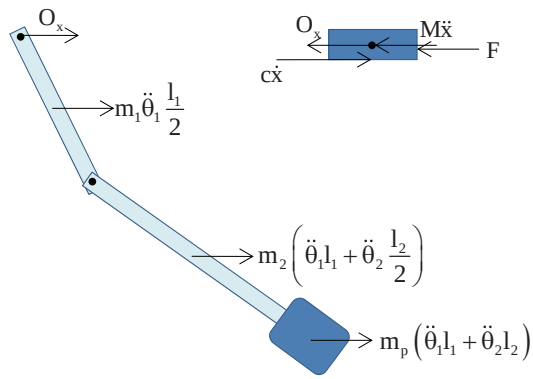

Figure 5 Free-body diagram showing all horizontal forces. ($M = m + m_1 + m_2 + m_p$ and O_x = force disturbance resulting from oscillations of the links and payload, l_1, l_2 = link lengths.)

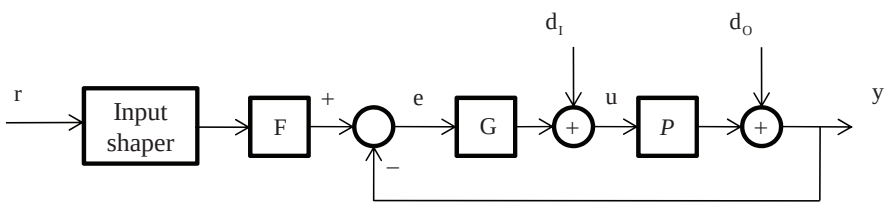

Figure 6 Closed-loop system block diagram consisting of an input shaper, a quantitative-feedback-theory-based controller (G), prefilter (F), r, e, u and y are the reference input, error, plant input and plant output, respectively and d_I and d_O are disturbances at plant input and output, respectively.

reduced and the payload displacement will closely approximate the slider displacement.

Considering the control-design plant model in Equation 7, without the disturbance O_x, a second-order transfer function is obtained as shown in Equation 8:

$$\frac{X(s)}{F(s)} = \frac{1}{Ms^2 + cs}, \quad (8)$$

where *M* and *c* are as defined previously and their values are given in Table 1. By allowing *M* and *c* to have ±10% variations from their nominal values, the transfer function (Equation 8) can be plotted on the Nichols chart as Figure 7. The 10% variations come from the difference between the simplified control design model (Equation 8) and the true model (Equation 6) representing the actual pendulum. At each frequency, there are four points; each represents one set of plant parameters. Note that for clarity, only five frequencies are displayed when the design includes more frequencies ranging from 0.1 to 100 rad.s^{-1}.

The design specifications are as follows. To effectively attenuate the inertia force disturbance O_x, set δ_{dI} = -15 dB in the plant-input disturbance rejection specification (Equation 3). To attenuate the plant-output disturbance, use δ_{dO} = 4 dB for the plant-output disturbance rejection specification (Equation 4). For tracking, use

$$\alpha = \frac{24.75}{s^2 + 10s + 25} \text{ and } \beta = \frac{101}{s^2 + 14s + 100}$$

in the tracking specification (Equation 5), where α and β are second-order transfer functions with appropriate step responses to be used as lower and upper bounds. In this case, the tracking lower-bound and upper-bound are arbitrary because there is no specific requirement on how the mass should move. The focus is on the vibration reduction of the payload. The lower and upper bounds are there to ensure that the whole assembly will move fast enough to see the effect of the payload vibration. All the specifications can be tightened as long as the control input is still within the saturation limit.

At a given frequency, each specification can be written as a bound on the Nichols chart. In this case, at a given frequency, there are three bounds from Equations 3–5. The intersection of these three bounds produces the strictest bound. The strictest bounds are shown in Figure 8 for various frequencies.

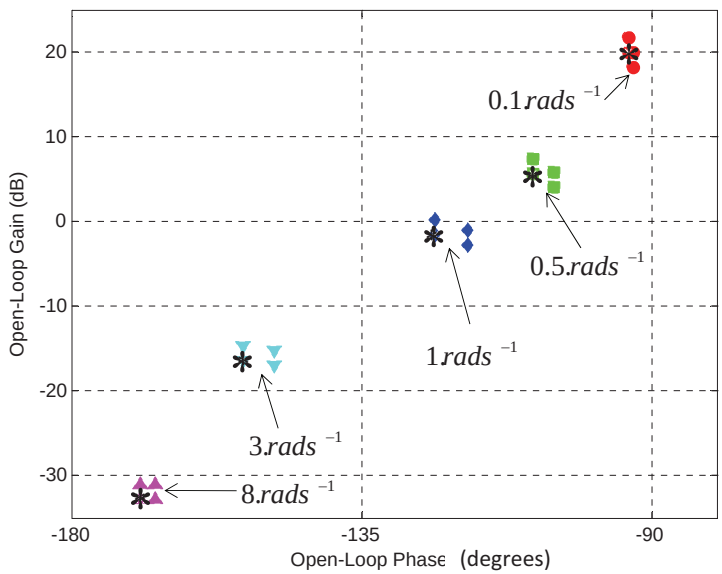

Figure 7 Plant templates at various frequencies. The asterisks mark the design point.

The final loop shape is the plot between loop gain |GP| and phase ∠GP after the controller G is designed. The controller G that satisfies all bounds is given by

$$G = \frac{1955.8085\,(s+1.616)}{(s+17.46)(s+29.17)}.$$

Since the prefilter F is outside-of–the-loop, it is designed to satisfy only the tracking bounds. The prefilter is given by

$$F = \frac{6.0688}{s+6.069}.$$

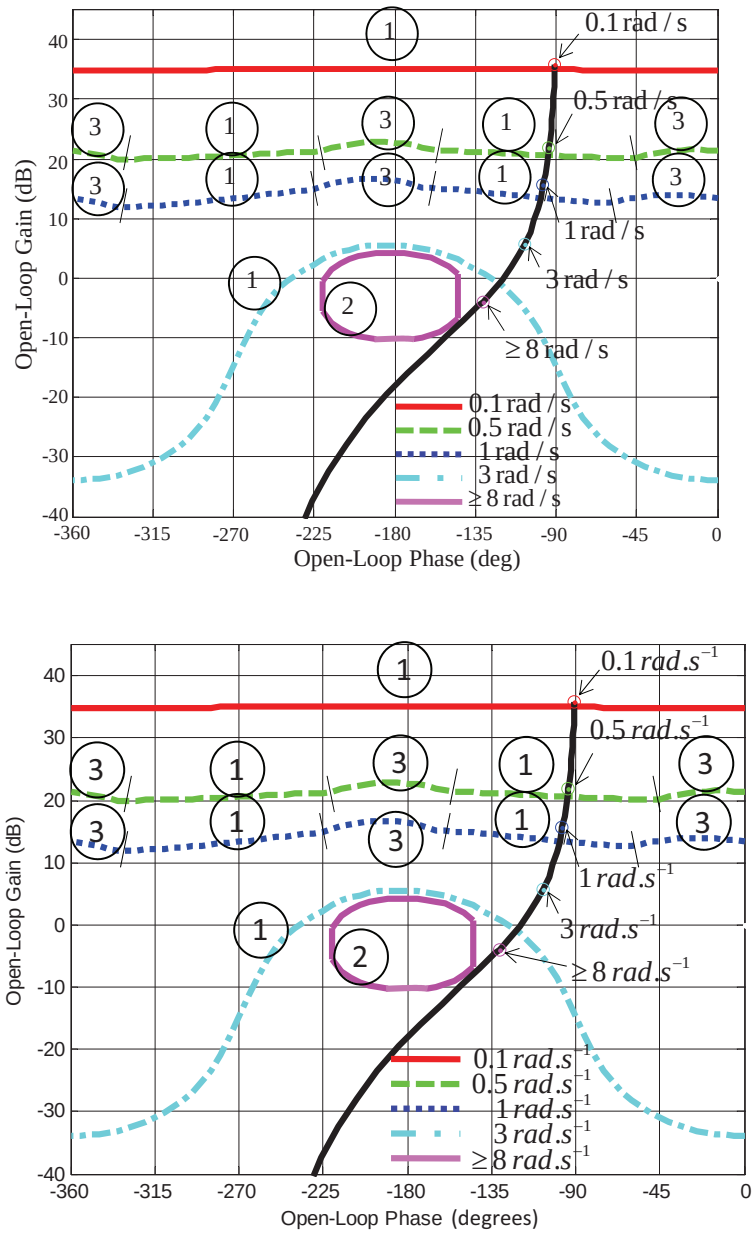

Figure 8 Specification bounds and final loop shape (The solid black line is the final loop shape, ① indicates the plant-input disturbance rejection bound, ② indicates the plant-output disturbance rejection bound and ③ indicates the tracking bound).

Simulation results with the simplified plant (Equation 8) are given in Figure 9. Figure 9a shows the magnitude of the transfer function from d_O to y whose maximum values are below the upper bound δ_{dO} for all plant variations. Figure 9b shows the magnitude of the transfer function from r to y whose values are within the bounds for all plant variations.

Figure 8 shows that the tracking specification is tightened at low frequencies (0.1–1 rad.s^{-1}) resulting in over design at 3 rad.s^{-1} and $\geq$ 8 rad.s^{-1}, which also shows in Figure 9b. This over design at high frequencies can be reduced at the expense of sacrificing the low-frequency specifications.

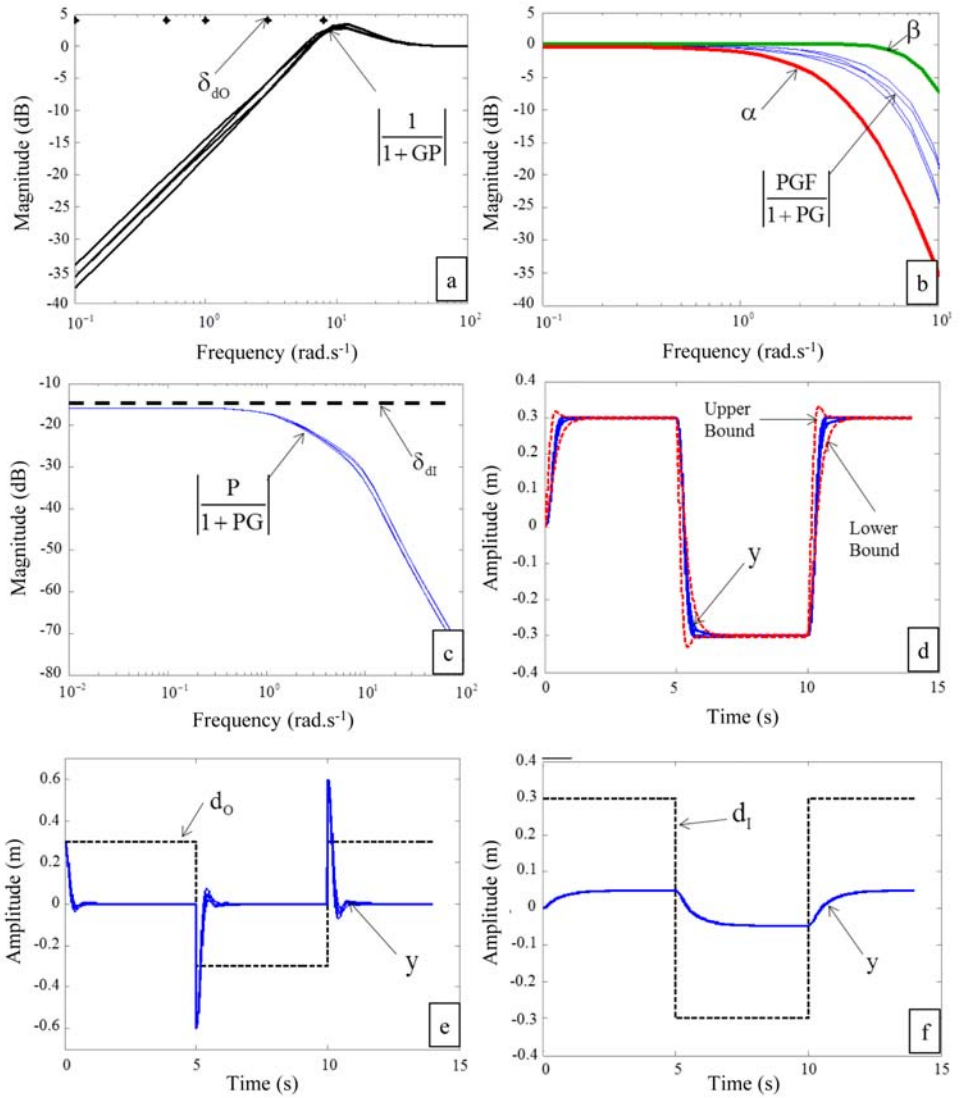

Figure 9 Frequency-domain and time-domain responses). P, G and F are the plant, controller and prefilter, respectively. y, d_I and d_O are the plant output, plant-input disturbance and plant-output disturbance, respectively. δ_{dO}, δ_{dI}, α, and β are the plant-output disturbance rejection specification, plant-input disturbance rejection specification, tracking specification lower bound and upper bound, respectively.

Figure 9c shows the magnitude of the transfer function from d_I to y, which is well below its bound δ_{dI}. Figure 9d, 9e and 9f present tracking, plant-output disturbance rejection and plant-input disturbance rejection responses in the time domain, respectively, when r, d_O and d_I are square waves with 0.3 m amplitude. It can be seen that all the outputs y from both d_O and d_I are attenuated substantially whereas the output y from the reference r is able to track the square wave within the pre-specified bounds.

Input shaper design

The input shaper requires the natural frequencies and damping ratios of the closed-loop system. Using the true model, with $\sin\theta \approx \theta$ and the controller and the prefilter obtained previously, the closed-loop natural frequencies and damping ratios can be computed. The natural frequencies of the underdamped modes are $\omega_1 = 2.83$ rad.s^{-1}, $\omega_2 = 6.82$ rad.s^{-1} and $\omega_3 = 17.1$ rad.s^{-1}. The corresponding damping ratios are $\xi_1 = 9.35\times10^{-2}$, $\xi_2 = 2.15\times10^{-1}$ and $\xi_3 = 8.13\times10^{-2}$.

Three impulses are used per one natural frequency and damping ratio. Three impulses were chosen to provide some robustness against uncertainties in the exact modes for the real system. Using more impulses results in greater robustness but with a slower response time due to the slower reference signal. The amplitudes and timing of the impulses can be found using Equations 1 and 2, where $t_1 = 0$ and $\hat{F}_1 = 1$ However, for the shaped input to have the same end point as that of the original reference input, the three impulses must sum to one, so the three impulses are scaled down accordingly. Three sets of three impulses are convolved together producing a final sequence of 27 impulses. This final sequence will be convolved with any incoming reference input to produce a shaped input that will minimally excite the closed-loop system natural frequencies, resulting in substantially less vibration.

The simulation results were obtained from implementing the control system in Figure 6 on the true model (Equation 6) of the two-staged pendulum, where the controller, the prefilter and the input shaper were designed previously. Figure 10 compares the payload position output, which is computed from x, θ_1, and θ_2 to be $x–l_1\theta_1–(l_1+l_2)\theta_2$, with a square-wave reference input. Figure **10**10a shows the QFT-based control being used but without input shaping, whereas Figure 10b shows the QFT-based control being used with input shaping. It can be seen that the payload vibration is reduced substantially as a result of moving the pendulum from point to point. The 3% settling time was also reduced from 17 to 4 s. Figure 11 shows the control input used in each case. The QFT-based control with input shaping used substantially less control effort but achieved

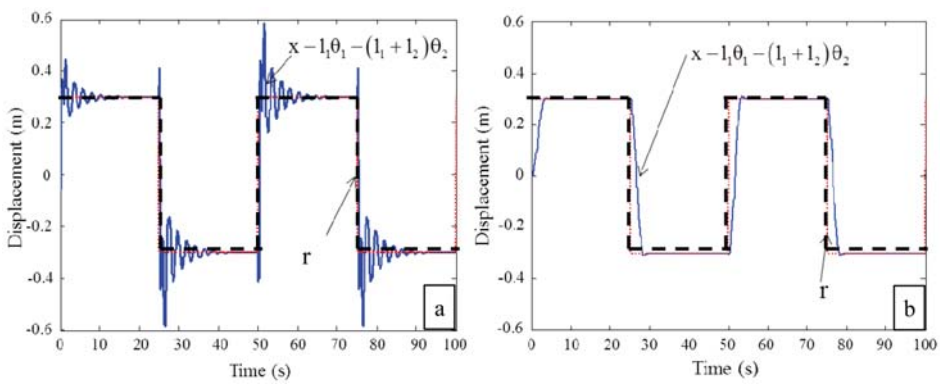

Figure 10 Payload position and its reference (r): (a) Quantitative feedback theory (QFT)-based controller without input shaping, (b) QFT-based controller with input shaping.

an even faster settling time than without input shaping.

The advantage of using QFT-based control together with input shaping is that the control system from the simplified second-order plant model can be designed with the swinging motion of both links and the payload being treated as force disturbances. The control system can be designed to reject the disturbances, thus reducing their detrimental effects on residual vibration.

RESULTS

Figure 12 provides a block diagram of the experimental arrangement. Two optical encoders measured the relative angular positions θ_1 and θ_2 of the links. Another optical encoder, attached to the motor, measured the motor shaft's angular position, which can be converted to the slider's linear position x. An uncertain payload container, carrying some movable coins, was placed at the tip. An accelerometer was attached near the payload to measure its linear acceleration.

A host computer, running Labview (National Instruments; Austin, TX, USA) and Matlab (Mathworks; Natick, MA, USA) software, was used to communicate with the user and a target computer. The impulse sequence was designed off-line using Matlab. The real-time hardware-in-the-loop experiment was performed using Labview.

A target computer contained two data acquisition cards whose functions were to acquire sensor signals and to send out actuator command from the control algorithm. One analog input (AI) channel, one analog output (AO) channel, and three counter channels were used in the experiment. The target operated using a Labview Real-Time operating system.

The host and target computers were connected to each other via a local area network line. A control signal was sent as voltage to a motor amplifier board to amplify to a level that could drive the direct current (DC) motor. An integrated circuit chip accelerometer was mounted at the tip to measure linear acceleration. A DC power supply provided current to the motor amplifier board.

A sampling time of 1 ms was used for the hardware. The closed-loop controller was described in the QFT-based controller design section, and the impulse sequence was described in the input shaper design section. However, in actual implementation, the impulse sequence must convolve in real-time with any incoming reference position command given by the human operator.

To do that, let IS(t) represent an impulse sequence of n impulses. It can be expressed in the time domain as Equation 9:

$$IS(t) = \sum_{i=1}^{n} A_i \delta(t - t_i),\ 0 \le t_i < t_{i+1} \quad (9)$$

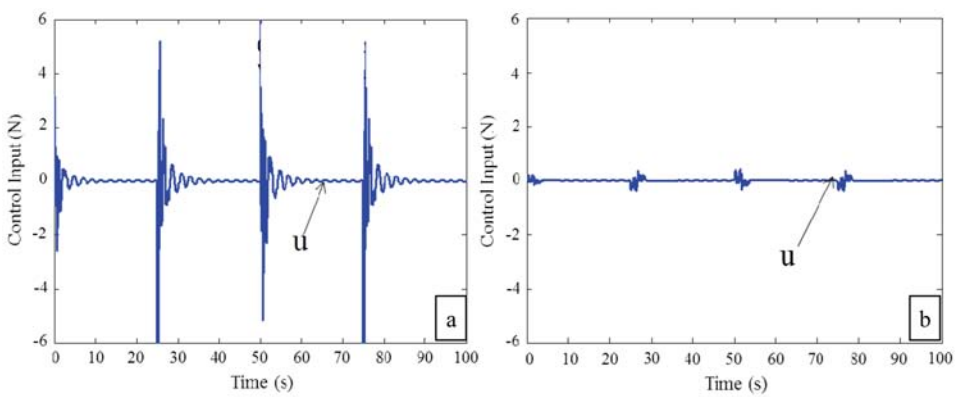

Figure 11 Control input: (a) Quantitative feedback theory (QFT)-based controller without input shaping, (b) QFT-based controller with input shaping. (u = Control input.)

where $\delta(t)$ is the Dirac delta function, A_i and t_i are the amplitude and time of the i^{th} impulse measured in meters and seconds, respectively. Suppose convolving this impulse sequence with a step reference input r(t) is needed. The convolution is given by Equation 10:

$$IS * r = \int_{-\infty}^{\infty} IS(\tau)\, r(t-\tau)\, d\tau \qquad (10)$$

Since $r(t-\tau) = r(-\tau + t)$ can be viewed as a mirror image of $r(\tau)$ about the vertical axis shifting by the amount of t, the convolution result can be obtained graphically as Figure 13. Figure 13a shows $IS(\tau)$ and $r(\tau)$. Figure 13b plots the mirror image $r(-\tau)$. Figure 13c shows $r(-\tau)$ shifted by t. Finally, Figure 13d shows the resulting convolution IS*r.

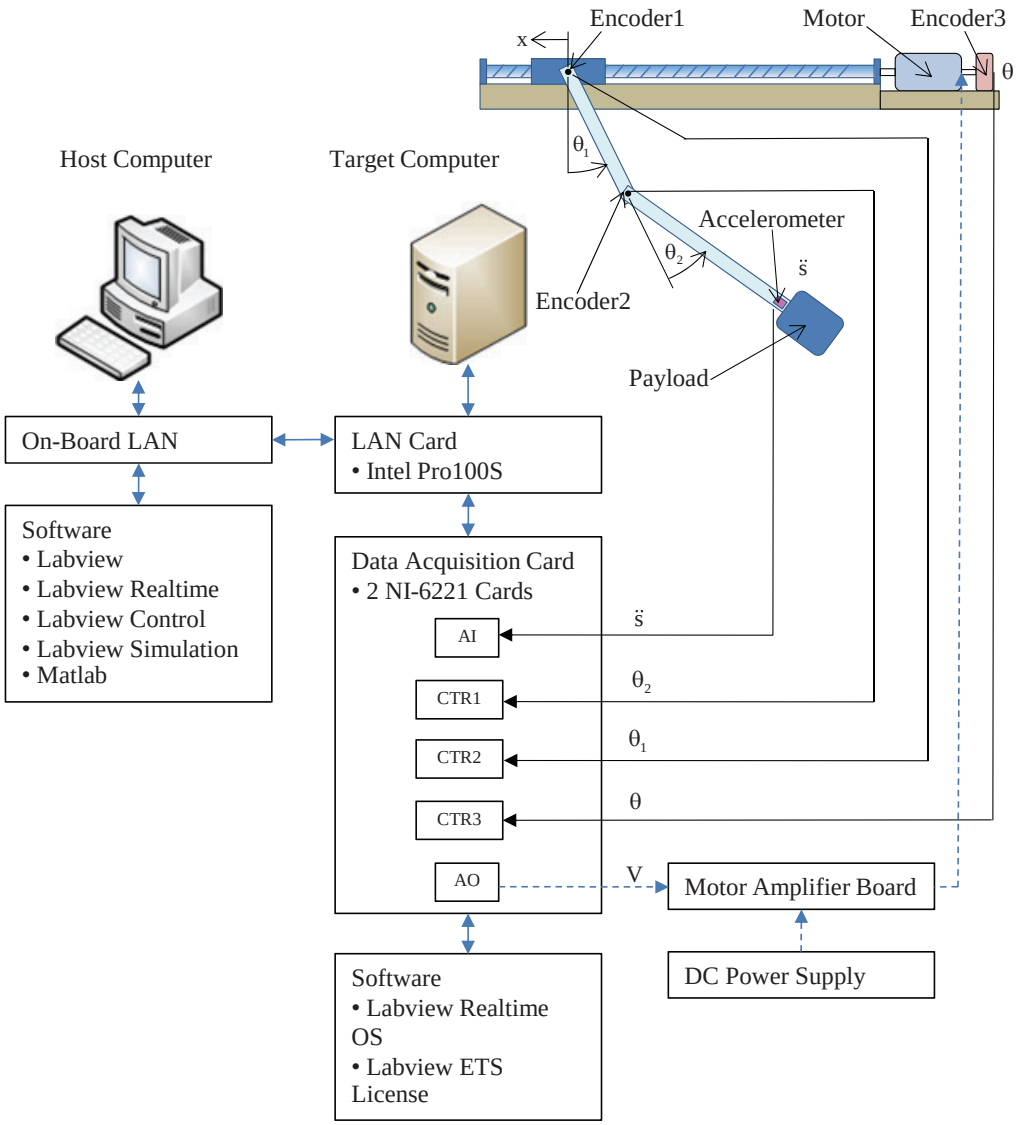

Figure 12 Diagram of the experimental setup. (LAN = local area network, AI = analog input channel, Ao = analog output channel, CTR1, CTR2, CTR3 = counter channels, $\ddot{s}$ = payload linear acceleration, θ_1 and θ_2 = relative angular positions of links, x = displacement coordinate, θ = motor angle and V = input voltage.)

The impulse sequence had 27 impulses spanning 450 time steps, when one time step equaled one sampling period of 0.01 s. In real-time convolution, 450 shift registers were added in the Labview program to store the current reference command $r(t_{current})$ as well as its previous 449 values. This reference command was given to the system in real-time by a human operator. A fixed array containing the impulse sequence was multiplied by the reference command stored in the shift registers. In this way, the most current command was multiplied by the first impulse, and the subsequent commands were multiplied by the subsequent impulses as shown in Figure 13c.

A toggle switch was written in the program to turn the input shaper on and off. A turntable knob was also added to the program to let an operator control the pendulum as desired. The readings from the knob were interpreted as the reference position to be followed by the pendulum's payload position.

Figure 14 plots the pendulum's payload position $(x–l_1\theta_1–(l_1+l_2)\theta_2)$ versus its desired trajectory given arbitrarily by the operator. By switching from the shaped to the unshaped reference inputs, it was clear that with the shaped input, the payload was able to settle faster with substantially less vibrations than in the unshaped case, which suffered from severe residual vibration. The experimental result of the input shaper was not as good as that of the simulation given in the input shaper design section because of the imperfection of the system identification in obtaining a dynamic model of the system.

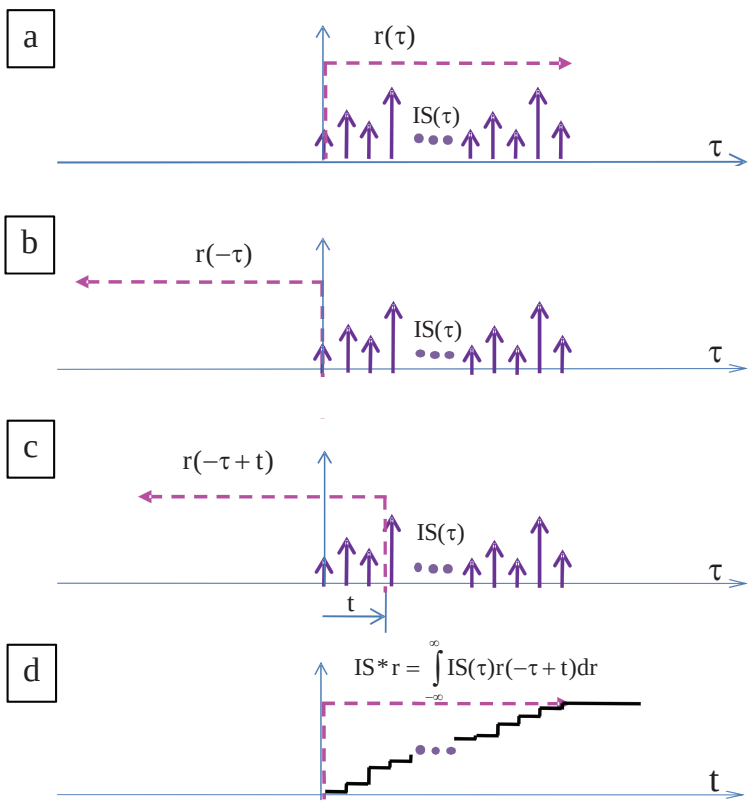

Figure 13 Graphical interpretation of the convolution process: (a) IS(τ) and r(τ); (b) plot of mirror image r(-τ); (c) shows r(-τ) shifted by t; (d) shows the resulting convolution IS*r. (r = Step reference input; IS = Input shaper impulse sequence; τ = Time, t = A specific time.)

Figure 15 shows the signal from the accelerometer at the tip, with substantially higher acceleration output during the unshaped period. The root-mean-square value of the acceleration was four times higher during the unshaped period than during the shaped period. Figure 16 contains the control input voltage to the motor amplifier. The control input had higher amplitude during the unshaped period.

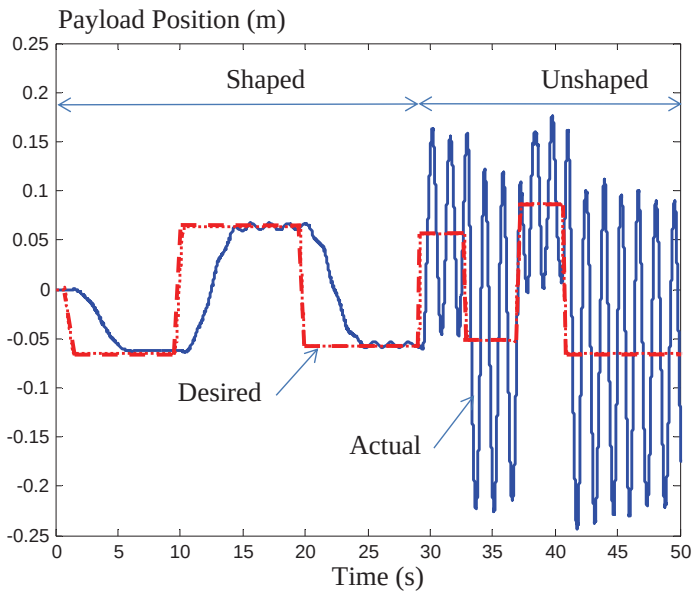

Figure 14 Tracking result for the shaped and unshaped cases (actual pendulum position = solid line, desired value = dashed line.)

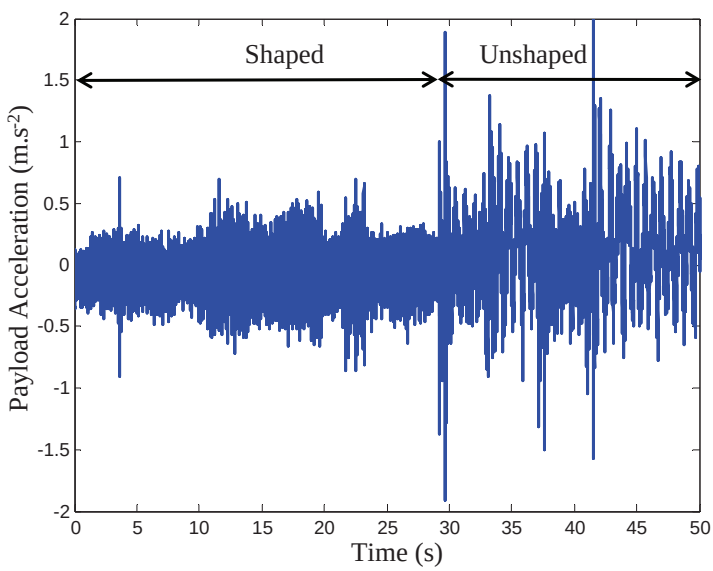

Figure 15 Payload acceleration for shaped and unshaped cases.

DISCUSSION

Some researchers have investigated placing the input shaper inside-of-the-loop, a so-called closed-loop signal shaper (CLSS.) Huey *et al.* (2008) reported that the CLSS could reduce noise-induced vibration and alleviate the detrimental effects caused by hard nonlinearity such as saturation and rate limit but a CLSS was not suitable for eliminating vibrations induced by plant-input and plant-output disturbances as well as by plant model uncertainty. Staehlin and Singh (2003) used the structure of the internal model controller for the closed-loop control without results on robustness. Kapila *et al.* (1999) applied a closed-loop controller based on the linear matrix inequality to a simulation problem. However, the controller is quite complicated and its use in practice is still limited. Because vibrations induced by disturbances and uncertainty are substantial, it is appropriate to put a controller inside-of-the-loop to attenuate the disturbances when uncertainty is present. Then, the input shaper can be placed outside-of-the-loop to create a shaped reference input for the resulting closed-loop system. The ability of the controller in attenuating the disturbances with pre-specified performance is vital for the proposed setting.

CONCLUSION

A control system consisting of a QFT-based controller, placed inside-of-the-loop, and an input shaper, placed outside-of-the-loop, delivered excellent results, both in simulation and in experiment, in reducing the oscillation of an uncertain payload of a two-staged pendulum, when the pendulum was commanded to move from point to point by a human operator. The QFT-based controller could be designed such that the effects from plant model uncertainties and external disturbances to the plant output were kept small and below pre-defined specifications. As a result, the vibration normally induced by these uncertainties and disturbances was reduced by the controller, so the input shaper could focus on attenuating the vibration induced by the reference input.

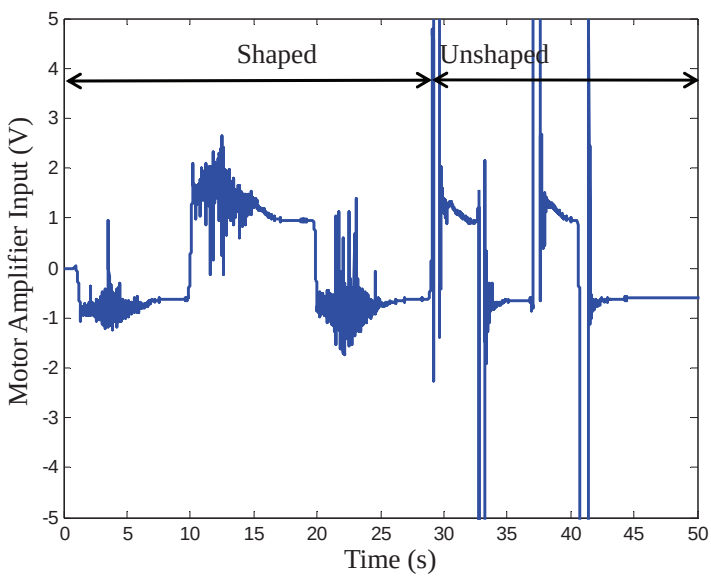

Figure 16 Control input to the motor amplifier for shaped and unshaped cases.

ACKNOWLEDGEMENTS

This work was performed at the Control of Robot and Vibration Laboratory, which is situated at and partially supported by the Research and Development Institute of Production Technology (RDiPT) of Kasetsart University, Thailand. The author would like to thank Mr. Craig Borghesani and Terasoft, Inc for the evaluation copy of the QFT Matlab toolbox.

LITERATURE CITED

Borghesani, C. 1993. **Computer Aided-Design of Robust Control Systems Using the Quantitative Feedback Theory.** MSc. Thesis, Mechanical Engineering Department, University of Massachusetts. Amherst, MA, USA.

Chatlatanagulchai, W., B. Inseemeesak and W. Siwakosit. 2008. Quantitative feedback control of a pendulum with uncertain payload. **Journal of Research in Engineering and Technology** 5: 45–71.

Franchek, M. and G.K. Hamilton. 1997. Robust controller design and experimental verification of I.C. engine speed control. **Int. J. Robust Nonlin.** 7: 609–628.

Garcia-Sanz, M. and J.X. Ostolaza. 2000. QFT-control of a biological reactor for simultaneous ammonia and nitrates removal. **Syst. Anal. Model. Sim.** 36: 353–370.

Garcia-Sanz, M. and F.Y. Hadaegh. 2004. Coordinated load sharing QFT control of formation flying spacecrafts 3D deep space and low earth Keplerian orbit problems with model uncertainty. *In* **NASA-JPL: Jet Propulsion Laboratory Document (D–30052).** Pasadena, CA, USA.

Horowitz, I. 1959. Fundamental theory of linear feedback control systems. **IRE Transactions on Auto Control** 4: 5–19.

_____. 1993. **Quantitative Feedback Design Theory (QFT).** QFT Publications. Boulder, CO, USA. 486 pp.

Houpis, C.H. and G. Lamont. 1992. **Digital Control Systems: Theory, Hardware.** 2nd ed. McGraw-Hill. New York, NY, USA. 752 pp.

Houpis, C.H. and P.R. Chander. 1992. Quantitative feedback theory and robust frequency domain methods. *In* **Symposium Proceedings at Wright Patterson Air Force Base.** Dayton, OH, USA.

Houpis, C.H., S.J. Rasmussen and M. Garcia-Sanz. 2005. **Quantitative Feedback Theory: Fundamentals and Applications.** 2nd ed. CRC Press. New York, NY, USA. 594 pp.

Huey, J.R. and W. Singhose. 2010a. Trends in the stability properties of CLSS controllers: A root-locus analysis. **IEEE Tran. Control Systems Tech.** 18(5): 1044–1056.

_____. 2010b. Design of proportional-derivative feedback and input shaping for control of inertia plants. **IET Control Theory Appl.** 6(3): 357–364.

Huey, J.R., K.L. Sorensen and W. Singhose. 2008. Useful applications of closed-loop signal shaping controllers. **Control Engineering Practice** 16: 836–846.

Kapila, V., A. Tzes and Q. Yan. 1999. Closed-loop input shaping for flexible structures using time-delay control, pp. 1561–1566. *In* **Proceedings of the 38th Conference on Decision and Control.** Institute of Electrical and Electronics Engineers. Phoenix, AZ, USA.

Karpenko, M. and N. Sepehri. 2004. QFT design of a PI controller with dynamic pressure feedback for positioning a pneumatic actuator, pp. 5048–5089. *In* J.L. Speyer, (ed.). **Proceedings of the American Control Conference.** American Automatic Control Council. Boston, MA, USA.

Pai, M.C. 2012. Robust input shaping control for multi-mode flexible structures using neuro-sliding mode output feedback control. **J. Franklin Inst.** 349: 1283–1303.

Phillips, S., M. Pachter and C.H. Houpis. 1995. A QFT subsonic envelope flight control system design. **Proceedings of National Aerospace Electronics Conference.** 1: 537–544.

Sating, R.R. 1992. **Development of an Analog MIMO Quantitative Feedback Theory (QFT) CAD Package.** MSc. Thesis. Graduate School of Engineering, Air Force Institute of Technology, Ohio, OH, USA.

Sidi, M. 2001. **Design of Robust Control Systems from Classical to Modern Practical Approaches.** 1st ed. Krieger Publishing Co. Malabar, FL, USA. 480 pp.

Singer, N.C. and W.P. Seering. 1989. Experimental verification of command shaping methods for controlling residual vibration in flexible robot, pp. 1738–1744. *In* **Proceedings American Control Conference.** American Automatic Control Council. Pittsburgh, PA, USA.

Singer, N.C. and W.P. Seering. 1990. Preshaping command inputs to reduce system vibration. **J. Dyn. Syst. Meas. Control** 112: 76–82.

Singhose, W., N.C. Singer and W.P. Seering. 1995. Comparison of command shaping methods for reducing residual vibration, pp. 216–221. *In* A. Isidori, (ed.). **Proceedings European Control Conference.** Rome, Italy.

Staehlin, U. and T. Singh. 2003. Design of closed-loop input shaping controllers, pp. 5167–5172. *In* G. Masada, (ed.). **Proceedings American Control Conference.** American Automatic Control Council. Denver, CO, USA.

Stergiopoulos, J. and A. Tzes. 2010. H_∞ closed-loop control for uncertain discrete input-shaped systems. **J. Dyn. Syst. Meas. Control** 132(4): 0410071–0410078.

Torres, E. and M. Garcia-Sanz. 2004. Experimental results of the variable speed, direct drive multipole synchronous wind turbine: TWT1650. **Wind Energy J.** 7: 109–118.

Yaniv, O. 1999. **Quantitative Feedback Design of Linear and Nonlinear Control Systems.** Kluwer Academic Publishers. Boston, MA, USA. 369 pp.

Zolfagharian, A., A. Noshadi, M.Z.M. Zain and A.R.A. Bakar. 2013. Practical multi-objective controller for preventing noise and vibration in an automobile wiper system. **Swarm and Evolutionary Computation** 8: 54–68.